

# Myocyte Shape Regulates Lateral Registry of Sarcomeres and Contractility

Po-Ling Kuo,\* Hyungsuk Lee,\*  
Mark-Anthony Bray,\* Nicholas A. Geisse,\*  
Yen-Tsung Huang,† William J. Adams,\*  
Sean P. Sheehy,\* and Kevin K. Parker\*

From the Disease Biophysics Group,\* Wyss Institute for Biologically-Inspired Engineering, and the Harvard Stem Cell Institute, School of Engineering and Applied Sciences, Harvard University, Cambridge; and the Department of Epidemiology,† Harvard School of Public Health, Boston, Massachusetts

**The heart actively remodels architecture in response to various physiological and pathological conditions. Gross structural change of the heart chambers is directly reflected at the cellular level by altering the morphological characteristics of individual cardiomyocytes. However, an understanding of the relationship between cardiomyocyte shape and the contractile function remains unclear. By using *in vitro* assays to analyze systolic stress of cardiomyocytes with controlled shape, we demonstrated that the characteristic morphological features of cardiomyocytes observed in a variety of pathophysiological conditions are correlated with mechanical performance. We found that cardiomyocyte contractility is optimized at the cell length/width ratio observed in normal hearts, and decreases in cardiomyocytes with morphological characteristics resembling those isolated from failing hearts. Quantitative analysis of sarcomeric architecture revealed that the change of contractility may arise from alteration of myofibrillar structure. Measurements of intracellular calcium in myocytes revealed unique characteristics of calcium metabolism as a function of myocyte shape. Our data suggest that cell shape is critical in determining contractile performance of single cardiomyocytes by regulating the intracellular structure and calcium handling ability. (*Am J Pathol* 2012, 181:2030–2037; <http://dx.doi.org/10.1016/j.ajpath.2012.08.045>)**

Cardiomyocytes contain parallel arrays of serially aligned and laterally registered sarcomeres that parallel the longitudinal cellular axis.<sup>1</sup> In healthy ventricles, the myocyte length/width ratio [ie, aspect ratio (AR)] in diastole is

tightly regulated, approximately 7:1.<sup>2–4</sup> When the heart undergoes concentric hypertrophy because of chronic pressure overload, myocytes increase cell width without a significant change in cell length, as new sarcomeres are added in parallel to existing sarcomeres, decreasing the myocyte AR.<sup>5,6</sup> When the heart progresses to failure, cardiomyocytes are elongated as new sarcomeres are added in series, without a significant change of cross-sectional area,<sup>4</sup> which can result in an increase of the myocyte AR to 11:1.<sup>3,4</sup> Because the sequel of these morphological changes is contractile dysfunction, it has been proposed by Gerdes and Capasso<sup>3</sup> that myocyte shape plays a direct role in regulating cardiac contractility.

Reduced myocyte contractility during heart failure is commonly attributed to altered protein phosphorylation, the result of complex changes in kinase and phosphatase expression and activity.<sup>7–9</sup> However, cytoskeletal structural anomalies, including intracellular coupling of sarcomeres, are also observed postmortem in the failing heart.<sup>10</sup> Myofilament disarray has played a critical role in the contractile impairment in the failing hearts.<sup>11,12</sup> Disruption in the Z-line contiguous registry, as observed in the ventricular muscle obtained from failing hearts,<sup>12</sup> may decrease the contractile force, suggesting an ultrastructural contributor to the disease. Based on our previous work,<sup>13,14</sup> we hypothesized that the changes in myocyte shape have a direct impact on their contractility and that this might be explained by how the sarcomeres are laterally registered within the myocyte.

## Materials and Methods

### Cardiomyocyte Culture

The described experiments were performed according to the *Guide of the Care and Use of Laboratory Animals*, pub-

Supported by a grant from the National Heart, Lung, and Blood Institute, NIH (R01HL079126 to K.K.P.), the Harvard Materials Research Science and Nanoscience Engineering Centers, and a United Negro College Fund–Merck Science Initiative postdoctoral fellowship (M.-A.B.).

Accepted for publication August 30, 2012.

Supplemental material for this article can be found at <http://ajp.amjpathol.org> or at <http://dx.doi.org/10.1016/j.ajpath.2012.08.045>.

Address reprint requests to Kevin K. Parker, Ph.D., 29 Oxford St, Pierce Hall, Room 321, Cambridge, MA 02138. E-mail: [kkparker@seas.harvard.edu](mailto:kkparker@seas.harvard.edu).

lished by the NIH (NIH publication 85-23, revised in 1996). All methods for handling laboratory animals were approved by the Animal Use and Care Committee at Harvard University (Cambridge, MA). Ventricular tissue was dissected from the hearts of 2-day-old Sprague-Dawley rats (Charles River Laboratories, Wilmington, MA). Ventricular tissue from the litters of approximately 10 pups was pooled during each cardiomyocyte isolation. These cardiomyocyte isolations were performed on a weekly basis, and the data for this study were collected from samples prepared over several weeks. The isolated tissue was homogenized and washed in HBSS and then digested with 0.1% trypsin and 0.1% collagenase for 14 hours at 4°C with agitation. Isolated myocytes were resuspended in M199 culture medium (Invitrogen, Carlsbad, CA) supplemented with 10% heat-inactivated fetal bovine serum, 10 mmol/L HEPES, 20 mmol/L glucose, 2 mmol/L L-glutamine, 1.5  $\mu\text{mol/L}$  vitamin B<sub>12</sub>, and 50 U/mL penicillin at 37°C and agitated. Immediately after purification, myocytes were plated on 25-mm-diameter glass coverslips that were coated by substrates with micropatterned fibronectin (FN) islands prepared as detailed later and kept in culture at 37°C with a 5% CO<sub>2</sub> atmosphere. Then, 100 mmol/L 5-bromo-2-deoxyuridine was added to the culture medium to prevent multiple nuclei formation. Immunostaining showed that >90% of cells plated from each cardiomyocyte isolation were positive for sarcomeric  $\alpha$ -actinin. Microscopic inspection revealed that the spontaneous contraction of the cardiomyocytes started approximately 3 days after isolation.

### *Patterning FN on Polyacrylamide Gels*

Micropatterned polyacrylamide gels were prepared by adapting the existing technique and the procedures.<sup>15–17</sup> In brief, a silicon wafer was spin coated with a layer of 10% by weight poly-N-iso-propyl acrylamide prepared in 1-butanol, followed by a 50- to approximately 75- $\mu\text{m}$  layer of photoresist (SU-8 2025; MichroChem Corp, Newton, MA), and treated by a standard photolithography procedure to obtain a master containing holes, with the designated ARs ranging from 1:1 to 11:1. The poly-N-iso-propyl acrylamide layer was dissolved by ice water to release the photoresist membrane. Polyacrylamide gels (5% acrylamide and 0.3% bis acrylamide, approximately 90  $\mu\text{m}$  thick, Young's modulus approximately 8 kPa measured by atomic force microscopy, as previously described<sup>18</sup>) containing 0.2- $\mu\text{m}$  fluorescence beads (Molecular Probes, Eugene, OR) were fabricated on 25-mm coverslips. The photoresist membrane was placed on the gel surface, and the holes of the membrane were filled by sulfo-sulfosuccinimidyl-6-4-azido-2-nitrophenylamino-hexanoate solution (Pierce, Rockford, IL), followed by UV light activation. After removal of excess sulfo-sulfosuccinimidyl-6-4-azido-2-nitrophenylamino-hexanoate solution, FN (100  $\mu\text{g/mL}$ ) was added to the membrane and was allowed to react with the photoactivated gel for 4 hours at 37°C to generate FN-coated adhesive islands. After removal of the photoresist membrane, the substrates were washed by PBS and immediately used for cell plating.

### *Patterning FN on Elastomers*

Polymer stamps designed for microcontact printing were prepared as previously described.<sup>19</sup> In brief, a complementary master pattern of 2- $\mu\text{m}$  photoresist (SU-8 2; MichroChem Corp) was generated on silicon wafers by standard optical lithography. The pattern consisted of rectangular shapes with a constant surface area of 2500  $\mu\text{m}^2$  and a variety of ARs, including 1:1, 2:1, 3:1, 5:1, 7:1, and 11:1. We found that 2500  $\mu\text{m}^2$  is the maximal area that neonatal rat cardiomyocytes can assume the designated shapes and be approximated as two-dimensional (2D) cells. Polydimethylsiloxane elastomer (Sylgard 184; Dow Corning, Midland, MI) was poured onto the photoresist master and cured. After peeling off, the polydimethylsiloxane elastomer formed a complimentary stamp of the master, and was inked with a 50  $\mu\text{g/mL}$  solution of FN for 1 hour at room temperature. Glass coverslips were spin coated with a thin layer of polydimethylsiloxane elastomer, cured, treated in a model 342 UVO cleaner (Jelight Company, Inc., Irvine, CA), immediately stamped by the FN-coated stamps for 5 minutes, and blocked in 1% F127 pluronic acid (BASF, Mount Olive, NJ). After 5 minutes, all stamped coverslips were washed in PBS and then immediately seeded with myocytes.

### *Substrate Deformation Measurement and Contractile Traction Force Analysis*

After 72 hours in culture, traction force measurements were conducted in spontaneously beating cardiomyocytes. To promote spontaneous beating, myocytes were incubated with culture medium containing 0.2  $\mu\text{mol/L}$  epinephrine for approximately 3 hours before traction force measurement. Only myocytes that assumed the desired shapes were used. For all myocytes sampled for contractility measurements ( $n = 22$ ), the mean value and SD of the beating frequency was  $1.1 \pm 0.5$  Hz. Coverslips containing the beating myocytes were removed from the incubator, mounted onto a custom-made microscope stage containing a bath chamber, and continuously perfused with 37°C normal Tyrode's solution (1 mmol/L HEPES, 5 mmol/L glucose, 1.8 mmol/L CaCl<sub>2</sub>, 1 mmol/L MgCl<sub>2</sub>, 5.4 mmol/L KCl, 135 mmol/L NaCl, and 0.33 mmol/L NaH<sub>2</sub>PO<sub>4</sub>, pH = 7.4; reagents from Sigma-Aldrich, St. Louis, MO). Fluorescence images of gels immediately beneath the mononucleated, contracting myocytes were taken at least for three contraction cycles at 28.1 Hz. Frame-to-frame bead displacements were measured as previously described.<sup>20</sup> This yielded a discretized 2D displacement field of the substrate with respect to the bead positions at the fully relaxed stage. The substrate deformation was assumed to be purely planar and was used to calculate the 2D contractile traction force field by adapting the established algorithm.<sup>15,21</sup> Briefly, the contractile traction force field was discretized by applying a lattice composed of  $4 \times 4$ - $\mu\text{m}^2$  squares to the cell interior, and solved from the displacement field

by the Boussinesq solution, assuming the substrate as an elastic half space with known mechanical properties. The Poisson ratio of the gel was assumed to be close to 0.5.<sup>17</sup> A 0-order Tikhonov regularization plus a constraint that the forces should not become exceedingly large was used to minimize and stabilize the solution. The  $L$  curve criterion was used to determine the optimal balance between the data agreement and the regularization, as previously described.<sup>21</sup> To quantitatively describe the contractile function of a single myocyte, we defined two coarse-grained variables,  $T_{x90}$  and  $T_{y90}$ , as the 90th percentile of the projection of the entire 2D traction force vectors along the  $x$ - and  $y$ -axes, respectively. Herein, we referred to the longitudinal cellular axis as the  $x$ -axis and the transverse axis as the  $y$ -axis. To represent contractility along different cellular axes, we further defined  $T_{x90max}$  and  $T_{y90max}$  as the  $T_{x90}$  and  $T_{y90}$  at the fully contracted state, respectively. We defined inherent contractility along each axis as maximal contractile stress per unit length by dividing  $T_{x90max}$  and  $T_{y90max}$  by cell length and width, respectively. To estimate how effectively the myocytes contract along the longitudinal axis, we calculated the ratio of the inherent longitudinal contractility/transverse contractility.

### Imaging Procedures

After 72 hours in culture, cardiomyocytes were fixed in 4% paraformaldehyde with 0.01% Triton X-100 in PBS buffer at 37°C for 15 minutes at room temperature and stained for sarcomeric  $\alpha$ -actinin (clone EA-53; Sigma-Aldrich). Tetramethylrhodamine-conjugated goat anti-mouse IgG (Alexa Fluor 594; Molecular Probes) was used for secondary staining, with chromatin stained by DAPI (Molecular Probes). All fluorescence and traction force measurement was performed with a Leica DMI 6000B microscope, using an  $\times 63$  plan-apochromat objective in the differential interference contrast mode. Images were taken only from those FN islands containing a single, mononucleated myocyte. For traction force experiments, images were collected with a Cascade 512B enhanced charge-coupled device camera, whereas immunofluorescence images were collected with a CoolSnap HQ charge-coupled device camera (both from Roper Scientific, Tucson, AZ) controlled by IPLab Spectrum (BD Biosciences/Scanalytics, Rockville, MD).

### ZLRL Measurement

We first normalized the sarcomeric  $\alpha$ -actinin stains to yield an image with a 0 mean and a variance of 1. The principal axis of variation at each pixel was computed from the gradient covariance of the normalized image to determine the orientation of the Z-line pixel. Individual Z-lines were identified as ridges in the image and were enhanced by applying Gabor filters to the image. These procedures produced a skeletonized image of line segments representing the Z-lines and an orientation image giving the local angles of individual Z-line pixels with respect to the short cellular axis. To eliminate the non-

striated portions of the  $\alpha$ -actinin stain, line segment vectors for which the mean orientation was  $>45^\circ$  (ie, not perpendicular to the long cellular axis) were excluded from subsequent analysis. This procedure also removed Z-lines associated with myofibrils spanning the short axis in low AR myocytes, because our analysis was restricted to the contractile contribution of myofibrils in the  $x$ -axis. A myofibril width of 0.7  $\mu\text{m}$  was taken as a threshold of Z-line registration length (ZLRL),<sup>22</sup> and line segments shorter than this value were discarded.

### Calcium Transient Measurements

Shape-controlled neonatal rat ventricular myocytes were incubated with 1.2  $\mu\text{mol/L}$  Fluo-4 AM (Invitrogen) and pluronic F-127 (0.1%; Invitrogen) for 15 minutes at 37°C. Myocytes were subsequently washed three times in Tyrode solution to remove dye residues. The myocytes were then placed under a 1-Hz field stimulation (7- to 12-V intensity), and Fluo-4 signals were monitored by line scan confocal microscopy (Zeiss LSM 5 LIVE Laser Scanning Microscope, Goettingen, Germany) with a  $\times 40$  oil immersion objective lens; a 488-nm wavelength laser was used to excite the dye, and signal was collected at  $>515$  nm. The scanning line was oriented transversely, across the width of the cell and away from the nucleus ( $>10$   $\mu\text{m}$ ) to monitor the cytosolic component of the calcium transients in high temporal resolution (500 Hz). Fluorescence signals were averaged along the cell width and normalized to be in the interval from 0 (minimum signal at diastole) to 1 (maximum signal at systole). Peak and decay times are defined as the time for the calcium signal to reach its peak value and then decay by 50%, respectively. To minimize the toxicity of Fluo-4, experiments were conducted for  $<1$  hour after dye loading.

### Statistical Analysis

All of the smoothing analyses were performed in R using the *mgcv* package (<http://www.r-project.org>). To compare the median and total ZLRL with respect to cell shape, the one-way analysis of variance test and multiple comparisons with the Scheffé criterion were performed. The level of significance was set at 5%.

### Results

We asked if myocyte shape affected myocyte contractility. When myocytes adhered to the FN-coated surface, they remodeled their shape to assume the shape of the FN island by reorganizing the cytoskeletal network. This allowed us to engineer myocytes with diastolic ARs of 1:1, 3:1, 5:1, 7:1, and 11:1 (Figure 1, A–E), where the diastolic AR was defined as the cellular AR at the fully relaxed state, and the systolic AR was defined as that at the fully contacted state, peak systole (Figure 1, F–J; see also Supplemental Videos S1 to S5 at <http://ajp.amjpathol.org>). The frame-to-frame substrate deformation is illustrated in Supplemental Videos S6 to S10 (available

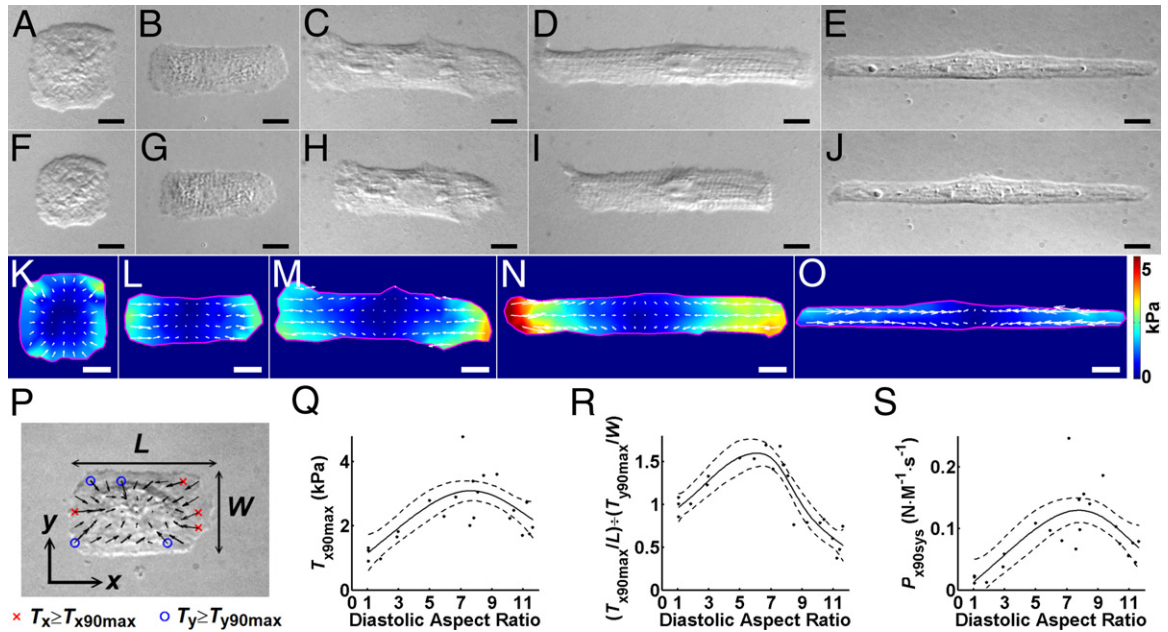


**Figure 1.** **A–E:** DIC images of myocytes of AR 1:1 (**A**), 3:1 (**B**), 5:1 (**C**), 7:1 (**D**), and 11:1 (**E**) at the fully relaxed state. **F–J:** DIC images of the myocytes of AR 1:1 (**F**), 3:1 (**G**), 5:1 (**H**), 7:1 (**I**), and 11:1 (**J**) at peak systole. **K–O:** Spatial maps of traction force at peak systole for the myocytes of AR 1:1 (**K**), 3:1 (**L**), 5:1 (**M**), 7:1 (**N**), and 11:1 (**O**). **Arrows,** traction force vectors; color scale, stress magnitude. To facilitate comparison, **K–O** have the same color scale at the right of **O**. Scale bars: 10  $\mu\text{m}$  (**A–O**). **P:** A DIC image of an AR 2:1 myocyte at the fully relaxed state, with the traction force vectors calculated at peak systole superimposed. Red crosses and blue circles, traction vectors with the  $x$  and  $y$  components at  $T_{x90\text{max}}$  and  $T_{y90\text{max}}$  or greater, where  $T_{x90\text{max}}$  and  $T_{y90\text{max}}$  represent the 90th percentiles of traction at peak systole projected along the  $x$ - and  $y$ -axes, respectively. **Q:**  $T_{x90\text{max}}$  as a function of cell ARs. **R:** The ratio of inherent longitudinal/transverse contractility as a function of ARs. **S:** The averaged power generation at systole as a function of ARs. **Q–S:** Solid lines, penalized regression spline with a thin plate regression spline as the basis; dotted lines, 95% CIs.

at <http://ajp.amjpathol.org>). During systolic frame-to-frame substrate deformation, the displacement vectors at the ends of the longitudinal cellular axis were directed inward, whereas the vectors at the middle of the cell pointed outward, perpendicular to the longitudinal axis, in accordance with Poisson's effect. These vectors then reversed direction during diastolic recoil. Once the systolic displacement of beads relative to their diastolic positions was determined, we computed the nominal stress field, assuming the substrate was linearly elastic, with the diastolic position as the reference state. This yielded the traction force map at peak systole (Figure 1, K–O), where the middle of the cell was spatially correlated with a region of relatively low stress, and high stresses were observed at the ends of the longitudinal cellular axis, with the observed maximal stress consistent with that previously reported.<sup>23</sup> Analysis of the traction stress as a function of cell shortening revealed hysteresis in contraction and relaxation cycles (see Supplemental Figure S1 at <http://ajp.amjpathol.org>). The five myocyte examples shown in Supplemental Figure S1 (available at <http://ajp.amjpathol.org>) exhibited similar temporal patterns in contraction and relaxation. If we plotted the  $T_{x90}$  as a function of time, both the  $T_{x90}$  (see Supplemental Figure S1A at <http://ajp.amjpathol.org>) and its time derivative (see Supplemental Figure S1B at <http://ajp.amjpathol.org>) exhibited similar temporal patterns across the five AR examples. The temporal profiles of the contracted and relaxed phases of  $dT_{x90}/dt$  were characterized as a rapid change followed by a slow decay, with a slightly longer latency in the relaxed phase. The maximal magnitude of

$dT_{x90}/dt$  in the relaxed phase was comparable to that of the contracted phase. The contracted phase latency of the five AR examples ranged from 106 to 213 milliseconds, the relaxed phase latency ranged from 142 to 320 milliseconds, and the time for  $T_{x90}$  to decay from the peak value to half maximum ranged from 106 to 142 milliseconds. Hysteresis between the contraction and relaxation cycles was observed in the stress-shortening plots of the entire beating cycles (see Supplemental Figure S1C at <http://ajp.amjpathol.org>).

Myocytes engineered to replicate the AR of healthy myocytes proved to exert the greatest tractional stresses at peak systole. We defined  $T_{x90\text{max}}$  and  $T_{y90\text{max}}$  as  $T_{x90}$  and  $T_{y90}$  at the fully contracted phase, respectively (Figure 1P). Data analysis revealed that, for all sampled myocytes, the maximal myocyte shortening was linearly correlated with the maximal longitudinal stress (see Supplemental Figure S2 at <http://ajp.amjpathol.org>). Figure 1Q showed how the maximal longitudinal stress varied depending on myocyte shape. The nonlinear  $T_{x90\text{max}}$ -AR association (Figure 1Q) was modeled using the penalized regression spline with a thin plate regression spline as the bases.<sup>24,25</sup> The 95% CIs for each mean value of the  $T_{x90\text{max}}$  were also plotted. The trend of the spline curve demonstrated that  $T_{x90\text{max}}$  was significantly dependent on cell AR ( $P = 0.0018$ ), because  $T_{x90\text{max}}$  increased monotonically as the AR increased from 1:1 to 7:1, but decreased thereafter. As depicted in Figure 1R, the ratio of longitudinal/transverse contractility similarly peaked at the myocyte ARs that mimic those of myocytes from healthy ventricles ( $P = 7 \times 10^{-6}$ ). To compare the

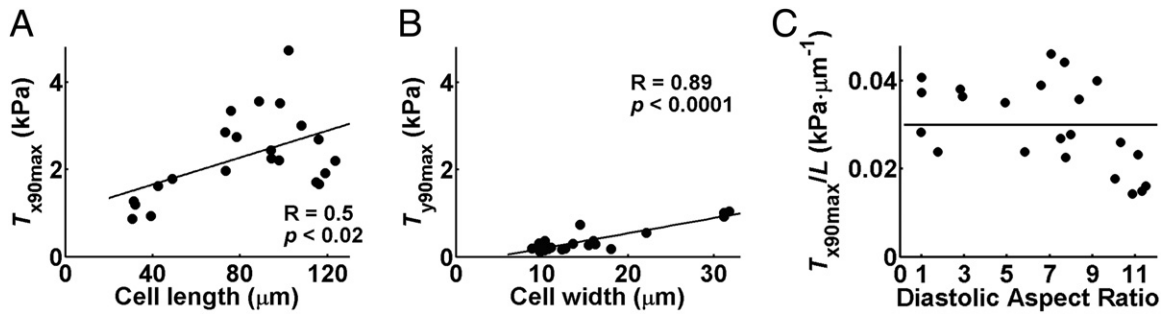


**Figure 2.** **A:** The relationship between maximal systolic  $T_{x90}$  and diastolic cell length. **B:** The relationship between maximal systolic  $T_{y90}$  and diastolic cell width. **C:** The  $T_{x90max}/L$  (ie, the inherent longitudinal contractility) as a function of ARs. Solid line, averaged inherent longitudinal contractility of all cells. **A** and **B:** The correlation coefficient,  $R$ , is determined by linear regression analysis, and a Student's  $t$ -test is applied for statistical analysis.

contractile efficiency, we computed the averaged power generation along the  $x$ -axis at systole,  $P_{x90sys}$ . The  $P_{x90sys}$  was significantly dependent on cell AR ( $P = 0.0029$ ), and the highest power occurred at ARs of approximately 7:1 to 8:1 (Figure 1S). The similar dependency of contractility on cell AR was observed in the analysis of DIC images of contracting myocytes (see Supplemental Figure S3 at <http://ajp.amjpathol.org>). Consistent with the traction force analysis, morphometric analysis also revealed that myocytes of medium ARs were optimized for contractility along the longitudinal axis. Analyzing acquired differential interference contrast images of contracting myocytes revealed that the cultured myocytes did not change their diastolic shape and size from beat to beat. This indicated that the substrates did not undergo plastic change and that the diastolic tension of the cultured myocytes was constant. Because the diastolic cellular size varied ( $853 \pm 255 \mu\text{m}^2$  for all sampled cells), the maximal myocyte shortening at the fully contracted phase was adjusted by the product of the cell length and width at the fully relaxed phase, and compared across different ARs (see Supplemental Figure S3A at <http://ajp.amjpathol.org>). To further examine the relationship between the adjusted maximal shortening and diastolic AR, we applied least-squares curve fitting with a second-order polynomial to the data. The normalized shortening depended on the diastolic ARs, increasing monotonically as the AR increased from 1:1 to 7:1, but decreasing at 11:1 (see Supplemental Figure S3A at <http://ajp.amjpathol.org>). The systolic AR was smaller than that at diastole, probably because of Poisson's effect in the transverse axis (see Supplemental Figure S3B at <http://ajp.amjpathol.org>). The increased systolic AR might substantially thicken the ventricular wall to help expel blood out of the chamber. Thus, the trend of the ratio of diastolic/systolic AR, as illustrated by the second-order polynomial curve fit in the inset of Supplemental Figure S3B (available at <http://ajp.amjpathol.org>), suggested that myocardium composed of medium AR myocytes might perform more effectively than one composed of myocytes of higher or lower ARs. Together, these data indicated that the contractility of single cardiomyocytes was optimized at the ARs observed in healthy ventricles.

The traction force fields revealed that the maximal contractile stress along different cellular axes was linearly correlated with the axis dimension.  $T_{x90max}$  was moder-

ately correlated with diastolic cell length (Figure 2A) (correlation coefficient  $r = 0.51$ ,  $P$  of correlation = 0.0156), whereas  $T_{y90max}$  (Figure 2B) was strongly correlated with diastolic cell width ( $r = 0.8875$ ,  $P = 3 \times 10^{-8}$ ). The inherent longitudinal contractility ( $T_{x90max}/L$ /individual cell length) of higher AR (ie,  $AR > 8$ ) myocytes was smaller than the average of all sampled cells (Figure 2C). This suggested that cardiomyocytes of abnormally high ARs might be inherently less contractile.

We hypothesized that variations in the lateral registry of sarcomeres could be a contributor to the differences in contractility with myocyte shape. To determine whether myofibril registry was altered as a function of cell shape, we analyzed the myofibril architecture in shape-controlled myocytes. As illustrated in Figure 3A, a typical sarcomeric  $\alpha$ -actinin stain of single, beating myocytes was characterized by periodically repeated, continuous Z-lines, plus the non-striated portions at the cellular ends, as described in previous studies.<sup>26</sup> We defined the ZLRL as the length of a continuous sarcomeric  $\alpha$ -actinin stain that traversed the cell width. To facilitate ZLRL measurement, we delineated the contiguous Z-lines from the sarcomeric  $\alpha$ -actinin stains using a modified ridge detection algorithm (Figure 3A) (the Matlab code from the reference can be accessed in "Peter's functions for computer vision" at <http://www.csse.uwa.edu.au/~pk/research/matlabfns>, last accessed October 23, 2012).<sup>27</sup> For all sampled myocytes, the registration length of the detected Z-lines exhibited a similar nonnormality of distribution, as the example shown in Figure 3B, with 90% of the ZLRLs in the range of 1 to approximately  $6 \mu\text{m}$ . Thus, the median ZLRL of individual myocytes was measured, averaged for each shape, and compared across different ARs. The data indicate that the median ZLRL varied with respect to cell shape (Figure 3C), but only those of AR 3:1 and 5:1 were significantly longer than that of AR 1:1 ( $P < 0.05$ , multiple comparisons with the Scheffé criterion). Because the myocyte area in the  $xy$  plane was designed to be identical for all ARs, we reasoned that the sum of the overall ZLRLs in individual myocytes provided a measurement of the total quantity of physically coupled sarcomeres along the longitudinal axis. Statistical analysis revealed that the total ZLRL of low AR myocytes was significantly less than that of medium AR cells, and myocytes of AR 5:1 and 7:1 possessed a

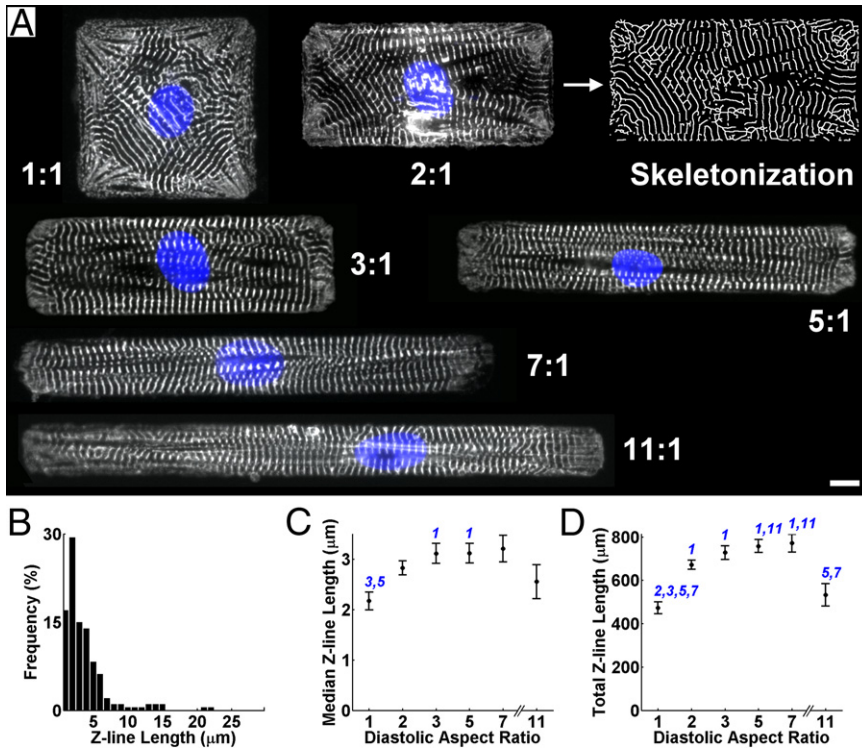


**Figure 3. A:** Sarcomeric  $\alpha$ -actinin (white) and DNA (blue) stains of myocytes with various ARs. An example of the skeletonized image of the AR 2:1 myocyte is also shown. Scale bar = 10  $\mu\text{m}$ . The frequency histogram of the detected Z-lines for the AR 2:1 cell shown in **A** is given in **B**, which exhibits an asymmetrical distribution as a function of the Z-line length. **C** and **D**: Mean and SD of the median and total Z-line registration length as a function of the diastolic AR, respectively. In **C** and **D**, the numbers above the error bars indicate the ARs whose means are statistically different ( $P < 0.05$ ) from the AR labeled. The sample size for each AR is as follows:  $n = 18$  (1:1),  $n = 29$  (2:1),  $n = 14$  (3:1),  $n = 15$  (5:1),  $n = 8$  (7:1), and  $n = 5$  (11:1).

significantly longer ZLRL in total than myocytes of AR 11:1 (Figure 3D). These data suggested that myocyte shape might play a role in optimizing the serial alignment and parallel coupling of sarcomeres.

The differences in contractility as a function of cell shape coincided with variations in the lateral registration of sarcomeres; however, depressed contractility in myocytes harvested from failing hearts was most often attributed to alterations in the amplitude and duration of cal-

cium transients.<sup>28–30</sup> We asked if we could detect similar variations in calcium handling as a function of myocyte shape. We measured calcium transients for myocytes with varied ARs using a confocal microscope. To control contraction frequencies of single myocytes, cells were electrically paced at 1 Hz using field stimulation, as demonstrated in the time course of calcium handling experiments using Fluo-4 (Figure 4A). The time to peak for the calcium transients was faster in cells with small ARs (ie,

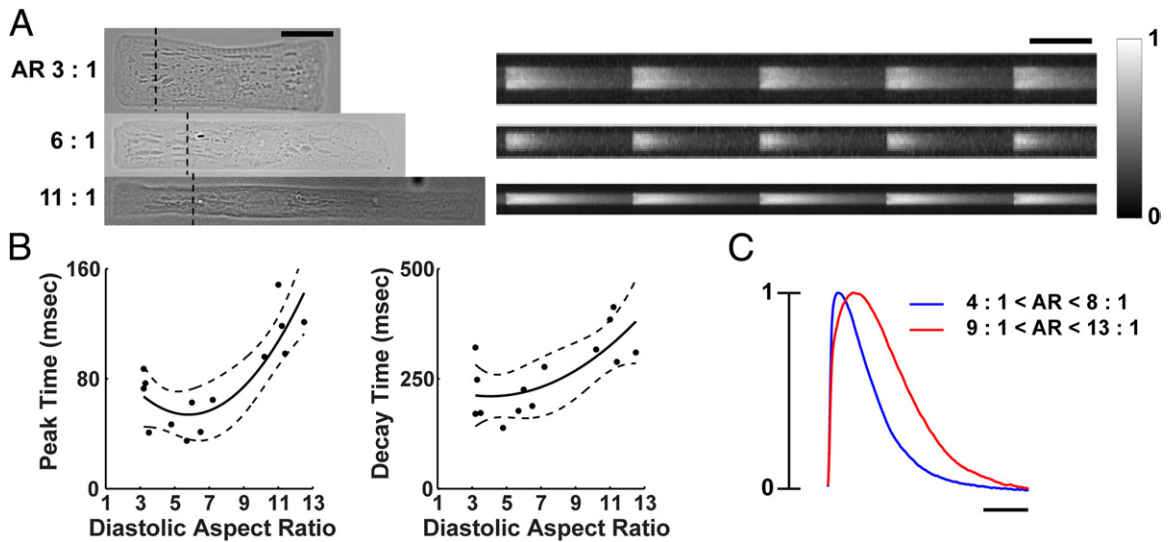


**Figure 4. Calcium handling as a function of cell shape. A:** Representative images of shape-controlled myocytes and their calcium transients. Fluo-4 signals for shape-controlled myocytes are monitored along the scanning lines (dotted line) using a confocal microscope. Scale bar = 20  $\mu\text{m}$  (DIC images). The time course of the Fluo-4 signal is normalized from 0 to 1 and used to analyze kinetic properties of the calcium transients. Scale bar = 0.5 seconds. **B:** Peak and decay times as a function of cell AR. Each data point, average values of five contraction cycles; solid line, a quadratic polynomial fit to the data; and dotted lines, 95% CIs (prediction). **C:** Normalized calcium waveforms are averaged for myocytes with medium (4:1 < AR < 8:1) and high (9:1 < AR < 13:1) ARs. Scale bar = 0.3 seconds.

<8) compared with those with high ARs (ie, >9) (Figure 4B). The minimum time to peak was observed in cells with a medium AR (ie,  $5 < \text{AR} < 7$ ). A fitted line through the data confirmed that the peak time depended on cell AR and increased significantly at high ARs. Similarly, increases in the decay time of the calcium transient were observed in cells with high ARs. A comparison of calcium waveforms across cells of varied AR revealed that calcium transients decayed more slowly in cells with high ARs relative to those with medium ARs (Figure 4C). These data were interesting, because they suggested that calcium metabolism within myocytes was distinctly sensitive to the shape of the cell.

## Discussion

Cardiomyopathies significantly affect the organization of myofibrils in cardiomyocytes.<sup>8</sup> In well-differentiated cardiomyocytes, adjacent myofibrils are tightly registered at the Z-lines, where the myofibrils are physically connected to the extracellular matrix, via the desmin filaments and costameres.<sup>31</sup> Contiguous Z-line registration across the cellular width effectively anchors the force vectors generated by individual myofibrils. Our data indicate that contractility of a single cardiomyocyte is correlated with myocyte shape, optimized at shapes resembling those found in healthy hearts, and decreases at shapes similar to those in failing hearts.

The work by Gerdes and colleagues,<sup>2-5</sup> >20 years ago, suggested a correlation between myocyte shape and contractile function and dysfunction in the healthy and failing heart. Our data support this hypothesis, drawing a direct correlation between myocyte shape and contractile strength. Our data further suggest that subcellular architecture (namely, the parallel registration of sarcomeric Z-lines) and calcium metabolism (specifically, the increase time of the calcium transient) are correlated with the range of myocyte shapes we engineered to mimic those studied by Gerdes. Subsequent work<sup>2-6</sup> since the Gerdes findings suggests that the cytoskeleton and sarcomeres play an important role in modulating ion channel kinetics and calcium metabolism.<sup>32-34</sup> Our findings of perturbations in Z-line registry between parallel sarcomeres suggest the importance of the parallel coupling of myofibrils in contraction. This is in agreement with our previous computational model of myofibrillogenesis, suggesting that the parallel coupling of myofibrils is important in maintaining the polarity of the contractile apparatus of a myocyte<sup>35</sup> and is consistent with the work, reviewed by Pyle and Solaro,<sup>36</sup> that the Z-lines are foci of signaling activity. Our data further suggest that the correlation of calcium signaling and contractile strength may depend on the ordered assembly of these foci into an intracellular network responsible for the spatiotemporal coordination of cellular contractility.

There are limitations in our experimental design. We chose neonatal cardiomyocytes rather than adult myocytes because of their ability to consistently (within approximately 48 hours) remodel their shape with respect to the geometric cues in the patterned matrix. Adult cardi-

omyocytes are slower to remodel their cytoskeleton in the current *in vitro* model and rarely assume the shape of the FN island in a timely manner. The addition of epinephrine to normalize the automaticity of a myocyte in the experimental protocol may influence the results, because exogenous catecholamines may alter myocyte contractility. Furthermore, our study focused primarily on evaluating the relationship between cardiomyocyte AR and systolic dysfunction, whereas the relationship between AR and diastolic dysfunction was not examined. However, the prolonged calcium transient durations observed in the high AR cardiomyocytes motivate us to further examine diastolic dysfunction in our *in vitro* model system because it was previously shown that prolongation of calcium transients was correlated with prolongation of diastole in rodent models of congestive heart failure.<sup>37</sup> Finally, our model approximates the 2D AR of myocyte shape, rather than the three-dimensional size. This is an important difference; however, our model is uniquely amenable to studies of the role of myofibrillogenesis in myocyte function because of its simplified myofibrillar architecture.

Our findings quantitatively relate the contractile function of myocytes with cell shape, intracellular structure, and calcium handling ability. These data are important, because they show how maladaptive remodeling of cellular and subcellular architecture may be a contributor to the reduced contractility of the failing heart.

## Acknowledgment

We thank Lauren E. Chin for help in data analysis.

## References

1. Sanger JW, Ayoob JC, Chowrashi P, Zurawski D, Sanger JM: Assembly of myofibrils in cardiac muscle cells. *Adv Exp Med Biol* 2000, 481:89-102
2. Gerdes AM: Cardiac myocyte remodeling in hypertrophy and progression to failure. *J Card Fail* 2002, 8:S264-S268
3. Gerdes AM, Capasso JM: Structural remodeling and mechanical dysfunction of cardiac myocytes in heart failure. *J Mol Cell Cardiol* 1995, 27:849-856
4. Gerdes AM, Kellerman SE, Moore JA, Muffly KE, Clark LC, Reaves PY, Malec KB, McKeown PP, Schocken DD: Structural remodeling of cardiac myocytes in patients with ischemic cardiomyopathy. *Circulation* 1992, 86:426-430
5. McCrossan ZA, Billeter R, White E: Transmural changes in size, contractile and electrical properties of SHR left ventricular myocytes during compensated hypertrophy. *Cardiovasc Res* 2004, 63:283-292
6. Sawada K, Kawamura K: Architecture of myocardial cells in human cardiac ventricles with concentric and eccentric hypertrophy as demonstrated by quantitative scanning electron microscopy. *Heart Vessels* 1991, 6:129-142
7. Belin RJ, Sumandea MP, Allen EJ, Schoenfelt K, Wang H, Solaro RJ, de Tombe PP: Augmented protein kinase C- $\alpha$ -induced myofilament protein phosphorylation contributes to myofilament dysfunction in experimental congestive heart failure. *Circ Res* 2007, 101:195-204
8. Hamdani N, Kooij V, van Dijk S, Merkus D, Paulus WJ, Remedios CD, Duncker DJ, Stienen GJ, van der Velden J: Sarcomeric dysfunction in heart failure. *Cardiovasc Res* 2008, 77:649-658
9. van der Velden J, Narolska NA, Lamberts RR, Boontje NM, Borbely A, Zaremba R, Bronzwaer JG, Papp Z, Jaquet K, Paulus WJ, Stienen GJ: Functional effects of protein kinase C-mediated myofilament phosphorylation in human myocardium. *Cardiovasc Res* 2006, 69:876-887

10. Hein S, Kostin S, Heling A, Maeno Y, Schaper J: The role of the cytoskeleton in heart failure. *Cardiovasc Res* 2000, 45:273–278
11. Perez NG, Hashimoto K, McCune S, Altschuld RA, Marban E: Origin of contractile dysfunction in heart failure: calcium cycling versus myofilaments. *Circulation* 1999, 99:1077–1083
12. Schaper J, Froede R, Hein S, Buck A, Hashizume H, Speiser B, Friedl A, Bleeze N: Impairment of the myocardial ultrastructure and changes of the cytoskeleton in dilated cardiomyopathy. *Circulation* 1991, 83:504–514
13. Bray MA, Sheehy SP, Parker KK: Sarcomere alignment is regulated by myocyte shape. *Cell Motil Cytoskeleton* 2008, 65:641–651
14. Parker KK, Tan J, Chen CS, Tung L: Myofibrillar architecture in engineered cardiac myocytes. *Circ Res* 2008, 103:340–342
15. Dembo M, Wang YL: Stresses at the cell-to-substrate interface during locomotion of fibroblasts. *Biophys J* 1999, 76:2307–2316
16. Pelham RJ Jr, Wang Y: Cell locomotion and focal adhesions are regulated by substrate flexibility. *Proc Natl Acad Sci U S A* 1997, 94:13661–13665
17. Wang N, Ostuni E, Whitesides GM, Ingber DE: Micropatterning tractional forces in living cells. *Cell Motil Cytoskeleton* 2002, 52:97–106
18. Engler A, Bacakova L, Newman C, Hategan A, Griffin M, Discher D: Substrate compliance versus ligand density in cell on gel responses. *Biophys J* 2004, 86:617–628
19. Tan JL, Liu W, Nelson CM, Raghavan S, Chen CS: Simple approach to micropattern cells on common culture substrates by tuning substrate wettability. *Tissue Eng* 2004, 10:865–872
20. Butler JP, Tolic-Norrelykke IM, Fabry B, Fredberg JJ: Traction fields, moments, and strain energy that cells exert on their surroundings. *Am J Physiol Cell Physiol* 2002, 282:C595–C605
21. Schwarz US, Balaban NQ, Riveline D, Bershadsky A, Geiger B, Safran SA: Calculation of forces at focal adhesions from elastic substrate data: the effect of localized force and the need for regularization. *Biophys J* 2002, 83:1380–1394
22. Korostyshevskaya IM, Maksimov VF, Markel AL, Filyushina EE, Shmerling MD, Yakobson GS: Peculiarities of myocardial structure in rats with hereditary hypertension reared by normotensive females. *Bull Exp Biol Med* 2001, 132:895–897
23. Balaban NQ, Schwarz US, Riveline D, Goichberg P, Tzur G, Sabanay I, Mahalu D, Safran S, Bershadsky A, Addadi L, Geiger B: Force and focal adhesion assembly: a close relationship studied using elastic micropatterned substrates. *Nat Cell Biol* 2001, 3:466–472
24. Wood SN: Modelling and smoothing parameter estimation with multiple quadratic penalties. *J R Stat Soc B* 2000, 62:413–428
25. Wood SN: Thin plate regression splines. *J R Stat Soc B* 2003, 65:95–114
26. Atherton BT, Meyer DM, Simpson DG: Assembly and remodelling of myofibrils and intercalated discs in cultured neonatal rat heart cells. *J Cell Sci* 1986, 86:233–248
27. Hong L, Wan Y, Jain AK: Fingerprint image enhancement: algorithm and performance evaluation. *PAMI* 1998, 20:777–789
28. Lindner M, Erdmann E, Beuckelmann DJ: Calcium content of the sarcoplasmic reticulum in isolated ventricular myocytes from patients with terminal heart failure. *J Mol Cell Cardiol* 1998, 30:743–749
29. Pogwizd SM, Schlotthauer K, Li L, Yuan W, Bers DM: Arrhythmogenesis and contractile dysfunction in heart failure: roles of sodium-calcium exchange, inward rectifier potassium current, and residual beta-adrenergic responsiveness. *Circ Res* 2001, 88:1159–1167
30. Ward ML, Crossman DJ, Loisel DS, Cannell MB: Non-steady-state calcium handling in failing hearts from the spontaneously hypertensive rat. *Pflugers Arch* 2010, 460:991–1001
31. Samarel AM: Costameres, focal adhesions, and cardiomyocyte mechanotransduction. *Am J Physiol Heart Circ Physiol* 2005, 289: H2291–H2301
32. Calaghan SC, Le Guennec JY, White E: Cytoskeletal modulation of electrical and mechanical activity in cardiac myocytes. *Prog Biophys Mol Biol* 2004, 84:29–59
33. Dyachenko V, Christ A, Gubanov R, Isenberg G: Bending of z-lines by mechanical stimuli: an input signal for integrin dependent modulation of ion channels? *Prog Biophys Mol Biol* 2008, 97:196–216
34. Prosser BL, Ward CW, Lederer WJ: X-ROS signaling: rapid mechano-chemo transduction in heart. *Science* 2011, 333:1440–1445
35. Grosberg A, Kuo PL, Guo CL, Geisse NA, Bray MA, Adams WJ, Sheehy SP, Parker KK: Self-organization of muscle cell structure and function. *PLoS Comput Biol* 2011, 7:e1001088
36. Pyle WG, Solaro RJ: At the crossroads of myocardial signaling: the role of Z-discs in intracellular signaling and cardiac function. *Circ Res* 2004, 94:296–305
37. Perreault CL, Bing OH, Brooks WW, Ransil BJ, Morgan JP: Differential effects of cardiac hypertrophy and failure on right versus left ventricular calcium activation. *Circ Res* 1990, 67:707–712